Available online at www.sciencedirect.com
ScienceDirect
Scripta Materialia 60 (2009) 13–16
Scripta MATERIALIA
www.elsevier.com/locate/scriptamat

Torque, power requirement and stir zone geometry in friction stir welding through modeling and experiments

A. Arora,[a] R. Nandan,[a] A.P. Reynolds[b] and T. DebRoy[a,*]

[a] Department of Materials Science and Engineering, The Pennsylvania State University, PA, USA
[b] Department of Mechanical Engineering, University of South Carolina, SC, USA

Received 10 July 2008; revised 13 August 2008; accepted 14 August 2008
Available online 26 August 2008

The torque, power requirement and stir zone geometry during friction stir welding of AA2524 aluminum alloy were modeled by solving the equations of conservation of mass, momentum and energy. The model predictions agreed well with the corresponding measured values for a wide range of welding speeds and tool rotational speeds when the heat transfer coefficient and the friction coefficient values were adjusted.

Keywords: Friction stir welding; Convection; Plastic deformation; Modelling; Aluminum alloys

Although several numerical models of friction stir welding (FSW) have been developed for the calculation of heat generation rate [1–3] and heat transfer and materials flow [3–14], their testing has, for the most part, been limited to comparison of the numerically predicted temperature vs. time plots with the corresponding experimental data. A rigorous validation of numerical models must include examination of model capabilities to predict several important features of FSW such as the torque, power needed for welding and the geometry of the stir zone as a function of important welding variables over a wide range of values. Here we show that the model predictions of the stir zone geometry, torque and energy agree well with the corresponding measured values when appropriate values of the heat transfer coefficient and the friction coefficient values are used.

Friction stir welds of AA2524 alloy plates, $6.4 \times 100 \times 610$ mm, were examined [15]. The nominal composition of the alloy in wt.% is Cu: 4–4.5, Mg: 1.2–1.6, Mn: 0.45–0.7, Zn: 0.15, Ti: 0.1, Si: <0.06, Fe: 0.12 and Al: rest [15]. The welding direction was perpendicular to the primary rolling direction of the plate. The tool shoulder diameter was 20.3 mm and the pin was 6.2 mm in length and 7.1 mm in diameter. The thread pitch on the pin was 0.794 mm/thread. A lead angle of 2.5° and axial pressure of 130.7 MPa were used for all welds.

The temperature and velocity fields were solved assuming steady-state behavior. The plastic flow in a three-dimensional Cartesian coordinate system is represented by the momentum conservation equation in indicial notation, with i or $j = 1$, 2 and 3, representing the orthogonal directions [5,8,14]

$$\rho \frac{\partial u_i u_j}{\partial x_i} = -\frac{\partial p}{\partial x_j} + \frac{\partial}{\partial x_i}\left(\mu \frac{\partial u_j}{\partial x_i} + \mu \frac{\partial u_i}{\partial x_j}\right) - \rho U_1 \frac{\partial u_j}{\partial x_1} \quad (1)$$

where u is the velocity, ρ is the density, μ is the non-Newtonian viscosity, U_1 is the welding velocity and p is the pressure. Viscosity was determined from flow stress and effective strain rate as described in the literature [16].

The pressure field was obtained by solving the following continuity equation iteratively with the momentum equations for incompressible single phase flow.

$$\frac{\partial u_i}{\partial x_i} = 0 \quad (2)$$

where u_i is the velocity of plastic flow. The steady single-phase energy conservation equations with reference to a co-ordinate system attached to the heat source may be represented as follows [5,7,8,14]:

$$\rho C_p \frac{\partial (u_i T)}{\partial x_i} = -\rho C_p U_1 \frac{\partial T}{\partial x_1} + \frac{\partial}{\partial x_i}\left(k \frac{\partial T}{\partial x_i}\right) + S_{in} + S_b \quad (3)$$

where T is temperature in K, C_p is the specific heat and k is the temperature-dependent thermal conductivity of the workpiece/tool. The term S_{in} represents the source term due to interfacial heat generation rate at the tool

* Corresponding author. Tel.: +1 814 865 1974; e-mail: debroy@psu.edu

1359-6462/$ - see front matter © 2008 Published by Elsevier Ltd. on behalf of Acta Materialia Inc.
doi:10.1016/j.scriptamat.2008.08.015

pin–workpiece interface and S_b is the heat generation rate due to plastic deformation in the workpiece away from the interface. The heat generated at the interface between vertical and horizontal surfaces of the tool pin and the workpiece may be defined as:

$$S_{\text{in}} = [(1-\delta)\eta\tau + \delta\mu_{\text{f}}P_{\text{N}}](\omega r - U_1 \sin\theta)\frac{A_r}{V} \tag{4}$$

where A_r is any small area on the tool pin–workpiece interface, r is the radial distance of the center of the area from the tool axis, V is the control-volume enclosing the area A_r, τ is the maximum shear stress at yielding and θ is the angle with the direction of movement of the tool, η is the mechanical efficiency, i.e. the fraction of deformational work converted to heat energy, δ denotes the spatially variable fractional slip between the tool and the workpiece interface, μ_{f} is the spatially variable coefficient of friction, ω is the angular velocity, P_{N} is the pressure on the surface. The symbol η indicates the fraction of the deformational work that is converted to heat [17]. Its value has not been experimentally determined for the conditions of FSW. A value of 0.9 was taken for η in the calculations. The fraction $(1-\eta)$ denotes the stored energy of cold work that is released upon annealing. The second term in Eq. (4) represents the rate of frictional work per unit volume that is converted to heat with 100% efficiency [18]. The maximum shear stress at yielding ($\tau = \text{yield strength}/\sqrt{3}$) is a function of temperature. The temperature-dependent yield strength values for AA2024 have been used due to unavailability of data for AA2524. These are both Al–Cu alloys with the same amounts of major alloying elements. Both contain 4.5 wt.% Cu, 1.5 wt.% Mg and 0.6 wt.% Mn and trace amounts of Fe and Si which differ in the two alloys. Both are precipitation-hardening alloys and derive their strengths from the formation of intermetallic Al–Cu–Mg precipitates. Because their compositions are nearly identical, and microstructures and strengthening mechanisms are exactly same, their temperature-dependent yield strength values are expected to be comparable [19]. The values of yield strength vs. temperature were obtained from measurements at low strain rates because data at high strain rates are not available. The following relation derived from data reported in literature [19] was used:

$$\begin{aligned}\text{Yield strength(MPa)} = {} & -2.628\times10^{3} + 2.585\times10^{1}T \\ & - 7.81\times10^{-2}T^{2} \\ & + 9.55\times10^{-5}T^{3} \\ & + 4.14\times10^{-8}T^{4}\end{aligned} \tag{5}$$

where T is Temperature in K. In Eq. (4) the applied radial pressure has been neglected in the computation because the experimental measurements of x-force values have been reported to be much smaller than the axial force [15]. An estimate of the heat generation rate due to plastic deformation per unit volume, away from the tool–workpiece interface, S_b, has been calculated as $\varepsilon\mu\Phi$ where Φ is given by:

$$\Phi = 2\sum_{i=1}^{3}\left(\frac{\partial u_i}{\partial x_i}\right)^2 + \left(\frac{\partial u_1}{\partial x_2}+\frac{\partial u_2}{\partial x_1}\right)^2 + \left(\frac{\partial u_1}{\partial x_3}+\frac{\partial u_3}{\partial x_1}\right)^2 + \left(\frac{\partial u_3}{\partial x_2}+\frac{\partial u_2}{\partial x_3}\right)^2 \tag{6}$$

and ε is an arbitrary constant [14]. The term $\mu\Phi$ represents the heat generation in fluids which have much lower viscosity. The symbol ε is used to scale down this heat generation term to fit into the context of high-viscosity plasticized materials and to confirm to the low value of the plastic deformational heat generation rate in FSW. A similar approach has also been used in the literature [2, 20].

A heat flux continuity at the shoulder–matrix interface yields [14]:

$$k\left.\frac{\partial T}{\partial z}\right|_{\text{top}} = \frac{\sqrt{(k\rho C_{\text{P}})_{\text{W}}}}{\sqrt{(k\rho C_{\text{P}})_{\text{W}}}+\sqrt{(k\rho C_{\text{P}})_{\text{T}}}}q_1 \quad \text{in the range } R_{\text{P}} \leqslant r \leqslant R_{\text{S}} \tag{7}$$

where k is the thermal conductivity, ρ is the density and C_{p} is the specific heat. The subscript W and T indicate workpiece and tool, respectively. R_P and R_S represent the tool pin and shoulder radius, respectively and q_1 represents the total rate of heat generation at the shoulder–workpiece interface. It is given by [14]:

$$q_1 = [\eta(1-\delta)\tau + \delta\mu_{\text{f}}P_{\text{H}}](\omega r - U_1 \sin\theta) \tag{8}$$

At the bottom surface, there is a backing plate and the heat transfer coefficient from the bottom of the workpiece is not the same as for free convection.

$$k\left.\frac{\partial T}{\partial z}\right|_{\text{bottom}} = h_{\text{b}}(T - T_{\text{a}}) \tag{9}$$

where h_{b} is the bottom heat transfer coefficient and T_{a} is the ambient temperature of 298 K. The heat transfer coefficient at the bottom face depends on the local temperature and is given by the following relation [14]:

$$h_{\text{b}} = h_{\text{b0}}(T - T_{\text{a}})^{0.25} \tag{10}$$

where h_{b0} is the heat transfer parameter for the bottom surface.

Velocities at the tool–workpiece interface have been defined in terms of tool translation velocity and the tool pin angular velocity:

$$\begin{aligned} u &= (1-\delta)(\omega r \sin\theta - U_1) \\ v &= (1-\delta)\omega r \cos\theta \end{aligned} \tag{11}$$

At all other surfaces, temperatures are set to ambient temperature (298 K) and the velocities are set to zero.

The trend of the reported data [21] on the extent of slip during cross-wedge rolling can be fitted in the following relation:

$$\delta = 0.2 + 0.6\times\left(1 - \exp\left(-\delta_0\frac{\omega}{\omega_0}\frac{r}{R_{\text{S}}}\right)\right) \tag{12}$$

where δ denotes the fraction-slip and δ_0 is a constant. δ ranges between 0.2 (when relative velocity is zero and close to sticking condition) and 0.8 (when relative velocity is high and close to sliding condition). δ_0 has no units and is adjusted to obtain the spatial distribution of slip such that torque and thermal cycle are close to experimental values. The symbol ω_0 is the reference value for the tool rotation speed (rpm), taken as 400 rpm and R_{S} is the radius of the tool shoulder.

Values of friction coefficient were calculated considering the relative velocity between the tool and the workpiece guided by previous work in the field of friction welding of steel bars. The trend of the reported friction coefficient [18] can be fitted in the following form:

$$\mu_f = \mu_0 \exp\left(-\delta \frac{\omega}{\omega_0}\frac{r}{R_S}\right) \quad (13)$$

where μ_0 is the highest value of friction coefficient, i.e., the value of the friction coefficient when there is no slip between the tool and the workpiece.

The heat transfer coefficient at the bottom surface of the workpiece, the friction coefficient and the extent of slip were adjusted to obtain good agreement between the predicted torque values and the corresponding experimental values. In Eq. (10) the value of h_{b0} was taken as $0.007\ \mathrm{W\,m^{-2}\,K^{-5/4}}$ to achieve the appropriate heat transfer at the bottom of the workpiece. The value of δ_0 in Eq. (12) and μ_0 in Eq. (13) were optimized to 3.0 and 0.65, respectively. The mechanical efficiency η in Eq. (4) is taken as 0.9. For the heat generation away from tool workpiece interface $\mu\varepsilon\Phi$, ε was taken as 0.1. Temperature dependent thermal conductivity, k and specific heat, C_p, were expressed as follows [19]:

$$k(\mathrm{Wm^{-1}K^{-1}}) = 2.582\times10^{1} + 3.8\times10^{-1}T + 2.9\times10^{-5}T^2 + 2.67\times10^{-7}T^3 \quad (14)$$

$$C_p(\mathrm{Jkg^{-1}K^{-1}}) = 9.293\times10^{2} - 6.2\times10^{-1}T + 1.4\times10^{-3}T^2 + 4.32\times10^{-8}T^3 \quad (15)$$

The differential equations of continuity and transport were solved using SIMPLE algorithm-based solution procedure [6].

The computed temperature and velocity profiles for various tool rotational speeds are shown in Figure 1. The plastically deformed region is shown by the computed velocity vector profile. This geometry of this region is in good agreement with the shape of the plastically deformed part of the workpiece. The numerically computed temperature levels shown are comparable to the experimentally measured temperature values for similar materials [22].

Figure 2a shows a comparison between the computed and the experimentally determined torque for various welding speeds. The torque, Q, is computed using the following relation:

$$Q = \oint_A \vec{r}_A \times (\vec{\tau}_t dA) \quad (16)$$

where r_A is the position vector of the area element with respect to the axis of tool rotation and τ_t is total shear stress at the tool–workpiece interface given by

$$\tau_t = [(1-\delta)\tau + \delta\mu_f P] \quad (17)$$

Figure 2a shows fairly good agreement between the computed and the experimental results of torque as affected by the welding speed. The exception is the experimental result at the lowest welding speed which seems to deviate somewhat from the simple, linear trend, perhaps due to non-linearities in the material parameters which are not accounted for in the simulation. Overall, however, the torque is relatively insensitive to the welding speed because the change in the welding speed does not affect the computed temperature field around the tool pin as much as the tool rotation rate. Evidence for decreasing torque with decreasing welding speed at constant rpm is found in the literature [23] and may be due to two contributing factors. Firstly, for a constant tool rotation rate and decreasing welding speed, the volume of material being deformed on each revolution decreases, hence the heat is generated in a smaller volume, and this in turn may lead to slightly higher temperatures and lower flow stress. This will lower the value of τ in Eq. (17). Secondly, lower welding speeds will reduce the convective cooling, resulting from slower movement into the relatively cooler material in front of the tool.

Figure 2b shows a comparison of the computed and the experimental weld power as the welding speed changes. Power is calculated by multiplying the computed torque with the corresponding relative velocity of the tool and the area

$$\int q_1 dA = \sum_A [(1-\delta)\eta\tau + \delta\mu_f P](\omega r - U_1 \sin\theta)dA \quad (18)$$

Figure 2b shows that the computed power does not change significantly with welding speed within the range of welding speed studied because the tool rotational speed was kept constant. The relative velocity between

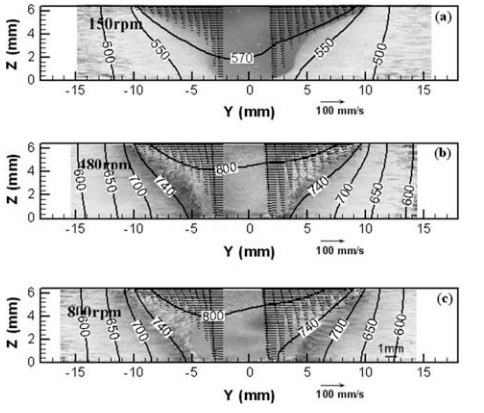

Figure 1. Relative comparison of the numerically computed temperature (K) and velocity profiles with the corresponding experimentally determined weld shapes [15]. The welding velocity was kept constant at $2.11\ \mathrm{mm\,s^{-1}}$ and the rotation speed was varied: (a) 150 rpm (b) 480 rpm and (c) 800 rpm.

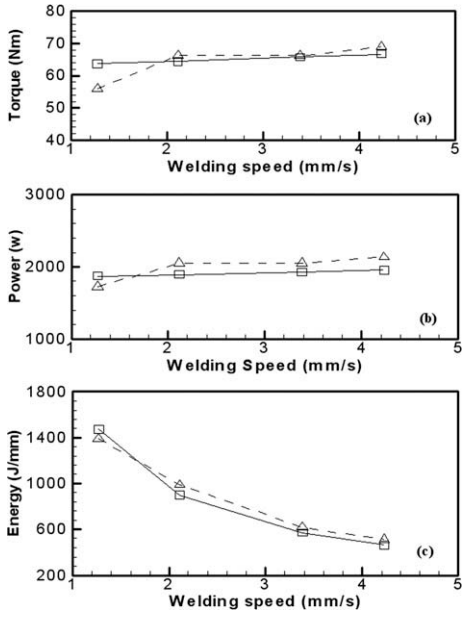

Figure 2. Variation of (a) torque, (b) power and (c) energy values with welding speed for the AA2524 friction stir welds where tool rotation speed is 300 rpm and axial force is 42.3 kN. The dashed line represents the experimental values reported by Yan et al. [15] and the solid line represents the numerically calculated values.

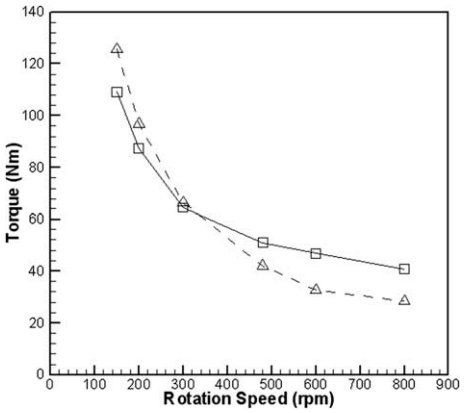

Figure 3. Torque values for the AA2524 friction stir welds with a welding speed is 2.11 mm s^{-1} and an axial force is 42.3 kN. The dashed line represents the experimental values reported by Yan et al. [15] and the solid line represents the numerically calculated values.

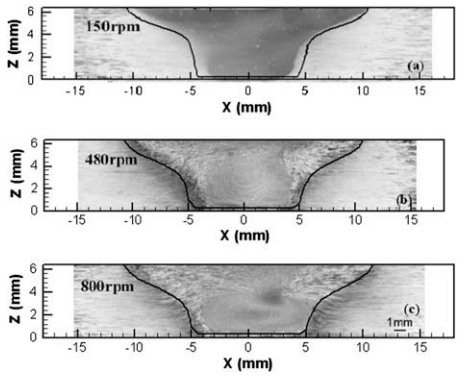

Figure 4. Relative comparison of the numerically computed TMAZ with the corresponding experimentally determined geometry [15]. The welding velocity was kept constant at 2.11 mm s^{-1} and the rotation speed was varied: (a) 150 rpm (b) 480 rpm and (c) 800 rpm.

the tool and the workpiece was determined mainly by the rotational speed and not by the welding speed.

The computed values of energy as a function of welding speed are shown in Figure 2c in comparison with the experimentally determined values of energy. The energy was computed by dividing the power by welding speed. The energy per unit length decreases with increase in welding speed because the energy is inversely proportional to the welding speed. The computed results show good agreement with the corresponding measured values.

The computed and experimentally measured torque values are shown in Figure 3. The computed torque decreases with increase in the rotational speed because it becomes easier for the material to flow at higher temperatures and strain rates. The form of the computed results agrees well with the corresponding experimental results.

The experimentally determined thermomechanically affected zones (TMAZ) are compared with the corresponding computed TMAZ in Figure 4. The computed TMAZ is determined by an iso-viscosity surface at 7×10^6 kg m^{-1} s^{-1}, above which there is no significant plastic deformation. Figure 4 shows that the computed TMAZ for different tool rotational speeds is in good agreement with the corresponding weld macro structures.

To conclude, the model can reliably predict the torque and power requirement for the friction stir welding of AA2524 alloy when appropriate values for friction coefficient and heat transfer coefficients are used. The torque required for the welding decreases with increase in the tool rotation speed due to higher heat generation rate and higher temperature. However, the torque is not significantly affected by the change in welding speed. The size of the TMAZ increases slightly with the increase in tool rotational speed due to higher power and higher peak temperatures.

This research was supported by a grant from the American Welding Society and Materials Division, Office of Naval Research, Johnnie DeLoach, Program Manager.

[1] M.Z.H. Khandkar, J.A. Khan, A.P. Reynolds, Science and Technology of Welding and Joining 8 (3) (2003) 165–174.
[2] H. Schmidt, J. Hattel, J. Wert, Modelling and Simulation in Materials Science and Engineering 12 (2004) 143–157.
[3] R. Nandan, T. DebRoy, H.K.D.H. Bhadeshia, Progress in Materials Science 53 (2008) 980–1023.
[4] P.A. Colegrove, H.R. Shercliff, Science and Technology of Welding and Joining 9 (6) (2004) 483–492.
[5] R. Nandan, B. Prabu, A. De, T. DebRoy, Welding Journal 86 (10) (2007) 313s–322s.
[6] R. Nandan, G.G. Roy, T. DebRoy, Metallurgical and Materials Transactions A 37A (2006) 1247–1259.
[7] R. Nandan, G.G. Roy, T.J. Lienert, T. DebRoy, Science and Technology of Welding and Joining 11 (5) (2006) 526–537.
[8] R. Nandan, G.G. Roy, T.J. Lienert, T. DebRoy, Acta Materialia 55 (2007) 883–895.
[9] G.G. Roy, R. Nandan, T. DebRoy, Science and Technology of Welding and Joining 11 (5) (2006) 606–608.
[10] T.U. Seidel, A.P. Reynolds, Science and Technology of Welding and Joining 8 (3) (2003) 175–183.
[11] M. Song, R. Kovacevic, Proceedings of the Institution of Mechanical Engineers, Part B: Journal of Engineering Manufacture 218 (1) (2004) 17–33.
[12] S. Xu, X. Deng, A.P. Reynolds, T.U. Seidel, Science and Technology of Welding and Joining 6 (3) (2001) 191–193.
[13] H.W. Zhang, Z. Zhang, J.T. Chen, Materials Science and Engineering: A 403 (1-2) (2005) 340–348.
[14] R. Nandan, T.J. Lienert, T. DebRoy, International Journal of Materials Research 99 (4) (2008) 434–444.
[15] J.H. Yan, M.A. Sutton, A.P. Reynolds, Science and Technology of Welding and Joining 10 (6) (2005) 725–736.
[16] T. Sheppard, A. Jackson, Materials science and technology 13 (3) (1997) 203–209.
[17] P. Rosakis, A.J. Rosakis, G. Ravichandran, J. Hodowany, Journal of the Mechanics and Physics of Solids 48 (3) (2000) 581–607.
[18] H.S. Kong, M.F. Ashby, Material Research Society Bulletin 16 (10) (1991) 41–47.
[19] E.A. Brandes, G.B. Brook, Smithells Metals Reference Book, seventh ed., Butterworth Heinemann, Oxford, 1999.
[20] A. Simar, J. Lecomte-Beckers, T. Pardoen, B. de Meester, Science and Technology of Welding and Joining 11 (2) (2006) 170–177.
[21] Z. Deng, M.R. Lovell, K.A. Tagavi, Journal of Manufacturing Science and Engineering 123 (4) (2001) 647–653.
[22] T. Long, W. Tang, A.P. Reynolds, Science and Technology of Welding and Joining 12 (4) (2007) 311–317.
[23] M.J. Peel, A. Steuwer, P.J. Withers, T. Dickerson, Q. Shi, H. Shercliff, Metallurgical and Materials Transactions A 37A (2006) 2183–2193.